JMATPRO	Journal of Advanced Materials and Processing 12 (46): 63-74, 2024 https://sanad.iau.ir/journal/jmatpro Doi: 10.71670/JMATPRO.2024.1229143

Research Paper

Continuous Ceramic Foam Production Through Direct Gas Injection Technology for High Temperature Refractory Materials

Hossein Ajamein[1], Leila Sharifi[2]*, Farnaz Assa[3], Seyed Hossein Mirhosseini[4]

1. Assistant Professor, Modern Ceramic Materials Institute, Academic Center for Culture, Education and Research-Yazd branch, Yazd, Iran
2. Assistant Professor, Modern Ceramic Materials Institute, Academic Center for Culture, Education and Research-Yazd branch, Yazd, Iran
3. Lecturer, Modern Ceramic Materials Institute, Academic Center for Culture, Education and Research-Yazd branch, Yazd, Iran
4. Assistant Professor, Modern Ceramic Materials Institute, Academic Center for Culture, Education and Research-Yazd branch, Yazd, Iran

ARTICLE INFO

Article history:

Received 23 December 2025
Revised: 11 January 2026
Accepted 26 January 2026
Available online 21 April 2024

Keywords:
Direct foaming
Porous ceramic refractories
Gas injection

ABSTRACT

Porous alumina is widely used as thermal insulation in high-temperature furnaces due to its desirable characteristics, including a high specific surface area, good permeability, low density, and low specific heat. Among the various fabrication routes, direct gas injection is considered one of the most cost-effective methods for producing alumina insulation foams. In this study, the properties of a commercial Goodfellow alumina insulation component were first examined as a reference to guide the development of a comparable product. A stable alumina slurry was prepared using Dolapix CE64 as the dispersant, and its stability was assessed. The optimal dispersant level was found to be 0.5 wt% relative to the solid content. The stabilized slurry, prepared with different solid loadings, was then introduced into the foaming device and aerated. Through a separate inlet, silica sol (4 wt%) and magnesium oxide (0.6 wt%) were added until the generated foam transitioned into a wet gel, which was subsequently dried and fired. The resulting porous bodies were sintered at 1400 °C for 2 hours and characterized using SEM, compressive strength testing, density measurements, and porosity analysis. The best foam properties were obtained from the slurry containing 78% solids, yielding a density of 0.92 g/cm³, compressive strength of 30 MPa, porosity of 78%, and thermal conductivity of 0.7 W/m·K—values that closely matched those of the reference material.

Citation: Ajamein, H.; Sharifi, L.; Assa, F.; Mirhosseini, S.H. (2024). Continuous Ceramic Foam Production Through Direct Gas Injection Technology for High Temperature Refractory Materials, Journal of Advanced Materials and Processing, 12 (46), 63-74. Doi: 10.71670/JMATPRO.2024.1229143

* *** Corresponding Author:**
E-Mail: sharifi.leila.jd@gmail.com

1. Introduction

Ceramic foams combine excellent chemical and thermal stability with low thermal conductivity and high surface area. These characteristics make them promising candidates for high-temperature insulation as well as catalyst supports and filters for molten metals [1, 2]. In porous ceramics, the size and size distribution of the pores, along with their interconnectivity and morphology, play a crucial role, as they determine properties such as mechanical strength, thermal conductivity, and gas or liquid permeability [3, 4]. The microstructure of porous ceramics is governed by their processing route and associated parameters [5]. Numerous processing techniques exist for fabricating porous ceramics, most of which can be categorized into one of the following approaches. In the replica method, a polymeric sponge is impregnated with a ceramic suspension, and after burnout of the organic template, an open-cell foam is obtained, where the cell size is defined by the structure of the original polymeric foam. In the fugitive phase method, a sacrificial pore former is used, often resulting in foams with highly ordered pore architectures once the pore former is removed. In the direct foaming method, a gaseous phase is dispersed and stabilized within a liquid, and depending on the processing parameters, either open- or closed-cell structures can be produced after drying and sintering [6-8]. A common feature of all these methods is that the introduced porosity significantly influences and modifies the mechanical properties of the resulting materials. Consequently, several mechanical testing techniques commonly used for dense ceramics may not be directly applicable to porous ceramics [9-11].

Interest in direct ceramic foaming has grown rapidly in recent years as advances in materials science have enabled new functionalities for ceramic foams. The literature reports numerous strategies aimed at improving both the structural integrity and performance of these materials. Direct foaming, one of the most versatile routes for fabricating ceramic foams, provides a simple, economical, and effective way to incorporate air bubbles into a powder suspension, allowing the pore structure to be readily controlled. However, foam slurries are inherently unstable at room temperature because of the thermodynamically unstable bubbles. This instability becomes even more pronounced in systems with high bubble content, where the slurry is highly susceptible to collapse and rupture, ultimately affecting the performance of the final product [12, 13].

Barg et al. developed an innovative direct foaming technique based on the emulsification of uniformly dispersed alkane or air–alkane droplets in a stable aqueous suspension of ceramic powders. Unlike conventional direct foaming, this approach generates foam through the evaporation of the emulsified alkane droplets, resulting in time-dependent expansion of the foam within a mold. The method enables the fabrication of interconnected structures with cell sizes ranging from 0.5 to 3 mm and porosities up to 97.5%. Moreover, the self-regulating foaming behavior provides significant flexibility in producing components with gradient structures or complex geometries. Foaming occurs as the alkane phase evaporates, expanding the stabilized droplets and increasing the overall volume of the foam. As a result, the green foamed body acquires a compact cylindrical shape conforming to the mold [14].

Capasso discussed two primary mechanisms for stabilizing air bubbles in ceramic matrices: surfactant-based stabilization and particle adsorption at the gas–liquid interface. The study emphasized the effectiveness of long-chain amphiphilic molecules—including lipids and proteins—in enhancing foam stability. However, it also highlighted the limitations of surfactants, which can lead to rapid foam destabilization, thereby requiring the use of setting agents to solidify the microstructure before bubble coalescence occurs. Capasso's findings underscore the importance of balancing bubble disproportionation with the setting rate of the suspension, demonstrating that porosity can be precisely tuned through careful control of processing parameters [15].

Building on this understanding, Werner and co-workers examined the freeze-foaming process as an alternative route for producing ceramic foams. This method eliminates the need for organic templates and demonstrates the versatility of ceramic foams for applications ranging from biomedical implants to thermal insulation. Their detailed analysis of the foam formation process revealed that the final structure is dictated by a complex interplay of material properties and processing variables. Critical factors such as air and water content, suspension temperature, and pressure-reduction rate were identified as key parameters for tailoring both the macro- and microstructure of the foams. This work not only advances the understanding of freeze foaming but also provides a framework for optimizing foam characteristics for specific applications [16].

Porous calcium hexaaluminate ceramics with spherical pores have also been fabricated using a direct foaming technique employing a high-speed electric mixer and calcium aluminate cement as the gelling agent. With increasing solid loading from 35% to 50%, the average pore size decreased from approximately 226 to 94 μm, the porosity decreased slightly from 85% to 82%, and the compressive

strength increased from 2.88 to 8.28 MPa [17]. Kirchhof investigated the mechanical behavior of foam materials, focusing on size effects in their elastic properties. The study highlighted the importance of specimen size in determining the mechanical response of foams—an issue of practical relevance for engineering design. Although significant advancements have been made in additive manufacturing and the design of cellular materials, experimental data on size effects in ceramic foams remain limited. Their work contributes a statistically robust dataset that enhances the understanding of mechanical reliability in ceramic foams and supports improved design practices [18].

As demonstrated in the literature, most previous studies have relied on high-speed mechanical stirring to aerate ceramic slurries. While this method is suitable for laboratory-scale production, it does not allow precise control of bubble or gas distribution in industrial settings [1, 19]. Therefore, in this study, a foaming device capable of mixing air and ceramic slurry in adjustable proportions was employed to produce ceramic foams via direct foaming. This system not only allows accurate control of the air content but also ensures a homogeneous distribution of air bubbles within the slurry.

2. Materials and Methods

2.1. Materials

In this study, α-alumina powder (Al_2O_3, AH221, 99.5%, Aria Arad Lian Faravar, Iran) was used to prepare the ceramic slurry. Dolapix CE64 was employed as a dispersing agent to stabilize the alumina particles within the suspension. Dolapix CE64, a polyacrylic compound, stabilizes the particles through an electrostatic mechanism. A stable silica sol containing 40 wt% silica (Isatis Nano Silica Company, Iran) was used as a binding agent. Polyvinyl alcohol (PVA) with a low molecular weight (7000 g/mol, Taiwan) was also utilized as an additional binder. Magnesium oxide was supplied by Dr. Mojallali Company, Iran.

2.2. Ceramic Foam Preparation

The samples were prepared using 70 wt% alumina powder and varying amounts of Dolapix CE64 dispersant from 0 to 0.7 wt% based on dry powder. The slurry preparation procedure was as follows: after dissolving Dolapix CE64 in distilled water for 15 minutes using a magnetic stirrer, alumina powder was added, and the mixture was further homogenized using a satellite mill to enhance uniformity. Milling was performed for 20 minutes at 200 rpm using aluminum grinding media. After determining the optimal dispersant concentration at different solid loadings under the above-mentioned conditions, the stability of the resulting slurries was evaluated. Subsequently, 0.5 wt% PVA was added to the slurry stabilized with Dolapix CE64, and the properties of the modified slurry were analyzed. In this study, a ceramic foam-generating device was designed and fabricated to produce porous alumina foams. The technical drawing of the device, along with its fabricated prototype, is presented in Fig. ***9***.

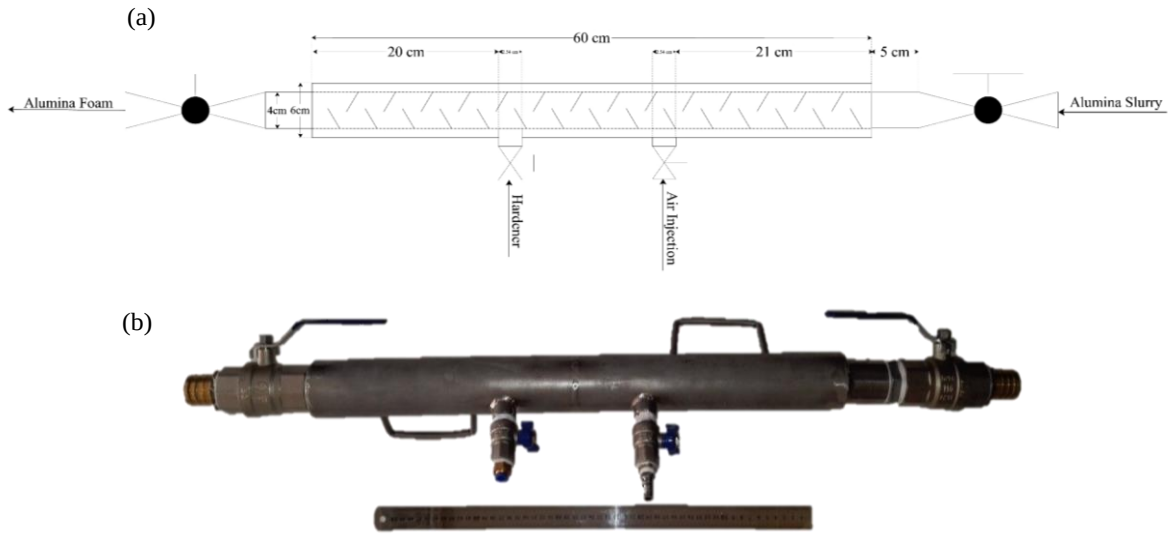

Fig. 9. (a) Technical drawing and (b) picture of the foaming machine

The designed device includes a slurry inlet, a compressed air inlet, a hardener inlet, and a foam outlet. The main tube of the device is approximately 60 cm in length and 6 cm in diameter. This tube has a shell-and-tube configuration, meaning that an inner tube is positioned within an outer shell, as shown in Fig. 9(a). Inside the inner tube, a series of 45° diagonal plates are arranged consecutively, creating flow resistance and slowing the movement of the slurry. While the outer shell is rigid, the inner tube is

constructed as a mesh structure. Both ends of the main tube contain inlet and outlet valves for the slurry and the resulting foam. At a distance of 21 cm from the inlet of the main tube, a compressed air valve injects air into the annular gap between the shell and the inner tube. The injected air is then forced through the perforations of the inner tube into the flowing slurry. This configuration ensures that air enters the slurry continuously along the length of the main tube, promoting both mixing and pore formation in the developing foam. Twenty centimeters above the bottom of the main tube, an inlet for the hardening agent is installed. This agent is introduced into the aerated slurry near the outlet of the tube, initiating the solidification process. The device can be mounted on a fixed base or operated as a portable unit. A slurry pump is used to deliver the slurry into the system, while a diaphragm pump injects the hardener. Compressed air required for bubble generation is supplied by an air compressor.

The slurry enters the foaming chamber under an air pressure of 0.3 MPa. Additionally, silica sol (4 wt%) and magnesium oxide (0.6 wt%) are added to the slurry. The mixture is then cast into polymer molds, and based on the characteristics of the final foamed components, the optimal sintering temperature was determined. To study the effect of solid loading, stable slurries containing 72, 75, 78, and 80 wt% solids were prepared and foamed under identical conditions (air inlet pressure of 0.3 MPa). All samples were sintered at 1400 °C, and their physical properties were subsequently evaluated. After approximately 2 hours, the green bodies were removed from the molds. Once demolded, the parts were still fresh and required complete drying to remove internal moisture. To prevent defects and cracking during drying, the samples were first kept at room temperature for one week, followed by drying in an oven at 120 °C for 5 hours. The sintering process was carried out at 1400 °C for 2 hours, with a heating rate of 3 °C/min. Fig. ***10*** illustrates the entire casting procedure used in this study.

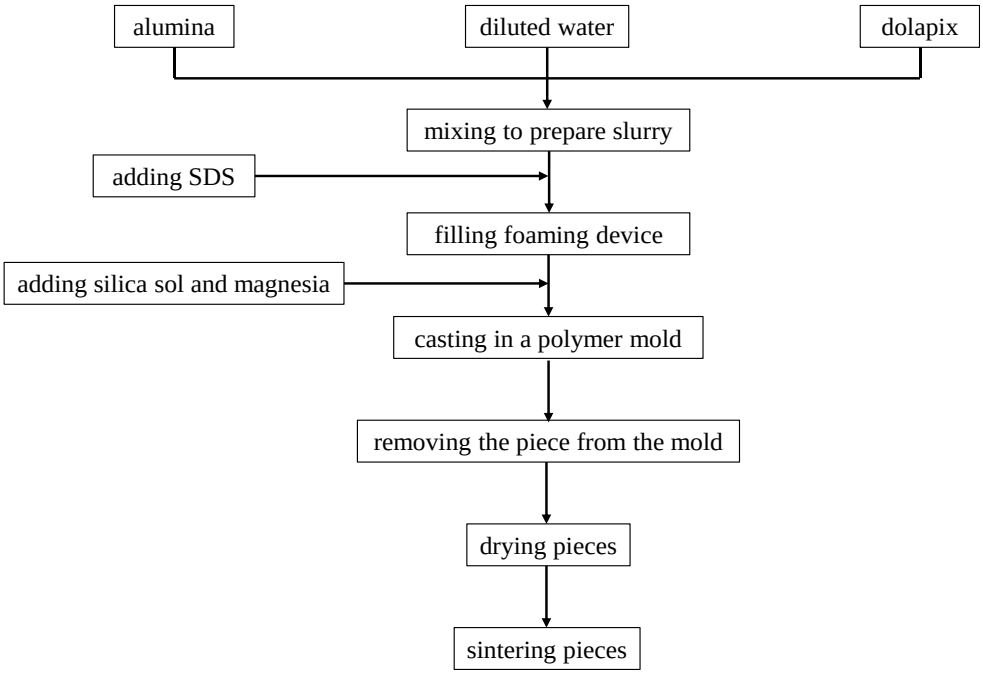

Fig. 10. Schematic of the aluminum foam manufacturing process

2.3. Characterization

Ten milliliters of each prepared suspension were poured into identical test tubes and allowed to stand undisturbed for 24 hours. After this period, the sediment was weighed, and the most stable suspension was identified. The sediment percentage was calculated using the Eq. (1).

$$\%sedimentation = \frac{sediment\ weight}{sediment\ weight + weight\ of\ suspended\ solids\ in\ the\ mixture} \times 100 \quad (1)$$

The total density of the samples in terms of g/cm^3 was calculated by dividing the weight of the parts by their volume. The percentage of total porosity was calculated using the Eq. (2).

$$P = 1 - \rho_r \quad (2)$$

Where ρ_r is the relative density and is calculated by the Eq. (3).

$$\rho_r = \frac{\rho_b}{\rho_{th}} \times 100 \quad (3)$$

ρ_{th} in the above equation is the theoretical density.

To examine the microstructure of the green samples, a scanning electron microscope (SEM), model StereoScan 360 (Leica/Cambridge), was used after gold coating. Both the surface and cross-sectional areas were analyzed directly on the fracture surfaces, without mounting or polishing. The compressive strength of the porous bodies was evaluated using cubic specimens measuring 10 mm on each side. The tests were performed using a 35-ton press machine (Seram Equipment) equipped with a Bong Shin load cell (Model DBBP-200). The loading rate was set at 0.0004 m/s.

2.4. Analyzes related to the reference sample

The X-ray diffraction pattern of the reference sample supplied by the Goodfellow Company is depicted in Fig. ***11***. All the peaks correspond to pure α-Al_2O_3 with good crystallinity (indicated by the presence of sharp peaks) and match the card number PDF # 0661-011-00. Moreover, the chemical analysis of the reference sample is listed in Table 1 which is consistent with the XRD results, confirming the high purity of alpha alumina in the reference sample.

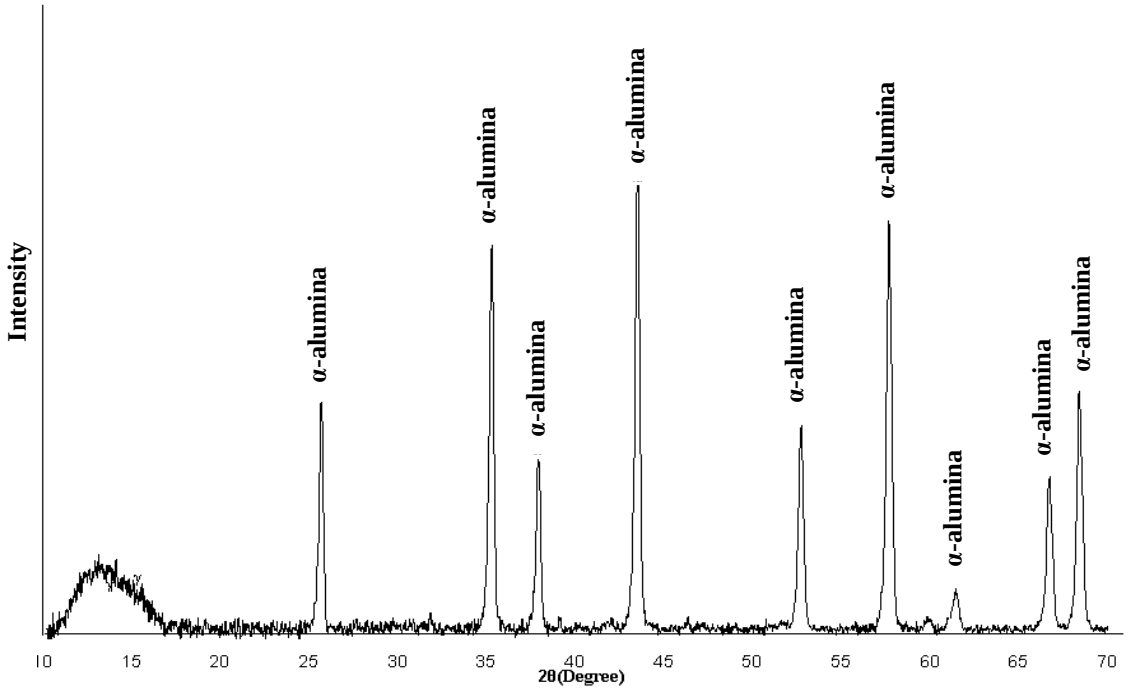

Fig. 11. X-ray diffraction (XRD) pattern of the reference sample

Table 1. Chemical analysis of the reference sample

Oxide	Composition (%)
Al_2O_3	99.6
SiO_2	0.01
Fe_2O_3	0.01
CaO	0.03
Na_2O	0.3

3. Results and discussion

Since the production of alumina foam with desirable properties requires a stable suspension with high solid content and low viscosity, it is essential to determine the optimal amount of dispersing agent.

3-1-Effect of pH

The pH of the dispersion medium significantly affects slurry stability. Hydrogen and hydroxyl ions exhibit high adsorption affinity for alumina particles, and their small ionic radius allows them to approach and bind to the particle surface. To prepare acidic slurries, nitric acid was used, whereas sodium hydroxide was employed to adjust alkaline pH. Fig. ***12*** shows the variation in sediment percentage after 24 hours as a function of slurry pH. It was observed that the sedimentation was lower under acidic conditions, indicating a reduced tendency for agglomeration and higher stability of the slurry in an acidic environment.

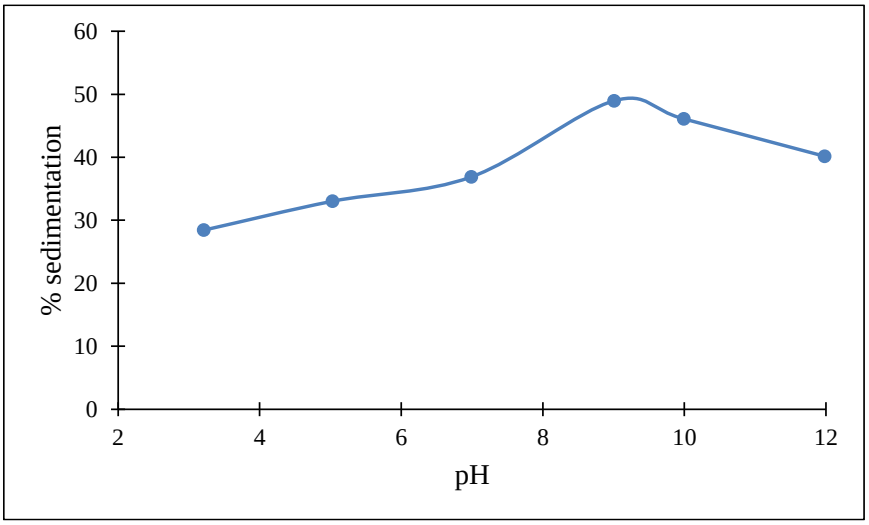

Fig. 12. Variation of sediment percentage with pH in slurries without dispersant

In slurries with acidic pH, alumina particles tend to adsorb H^+ ions from the medium, resulting in a positively charged particle surface. At the isoelectric point (IEP, pH ≈ 9), the surface charge of the alumina particles is zero. Under these conditions, electrostatic repulsion between particles is absent, and Van der Waals forces dominate, causing the particles to aggregate. As shown in Fig. ***13***, moving away from the IEP increases the zeta potential, which raises the energy barrier for flocculation. Consequently, slurries prepared under acidic conditions exhibit higher stability.

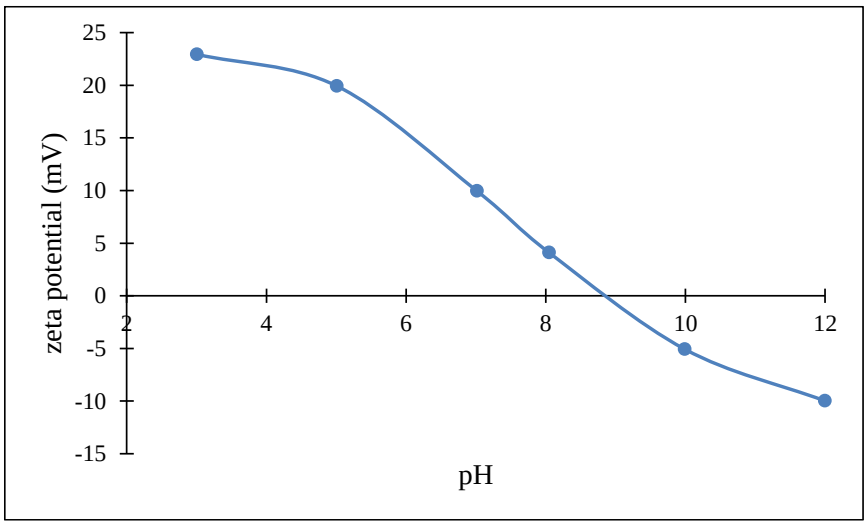

Fig. 13. Variation of zeta potential with pH for slurries without dispersants

3-2- Effect of pH

Although pH plays a significant role in the dispersion of alumina particles, sedimentation of the slurry due to particle agglomeration under gravitational force remains relatively high. Therefore, the use of a dispersant is necessary to improve slurry stability. In this study, Dolapix CE64 was employed as a dispersant. Dolapix CE64 is a polyacrylic compound that stabilizes particles primarily through electrostatic interactions. Adsorption of Dolapix CE64 on the surface of alumina particles increases the surface charge, enhancing repulsion between particles and thus improving slurry stability.

The zeta potential of slurries containing 0.5 wt% Dolapix CE64 at different pH values is presented in Fig. 14. Comparison of Fig. 13 and Fig. 14 shows that the presence of Dolapix CE64 shifts the isoelectric point (IEP) from pH 9 to pH 4. At pH 4, the particle surface carries no net charge, allowing Van der Waals forces to dominate and induce particle aggregation. As pH increases, the zeta potential becomes more negative due to the predominance of the surface charge provided by the dispersant. At pH 7, the zeta potential reaches -31 mV, indicating suitable dispersion and stability. Moreover, higher pH values were avoided to prevent corrosion of the foam tube; thus, pH 7 was selected as the optimal condition for subsequent experiments.

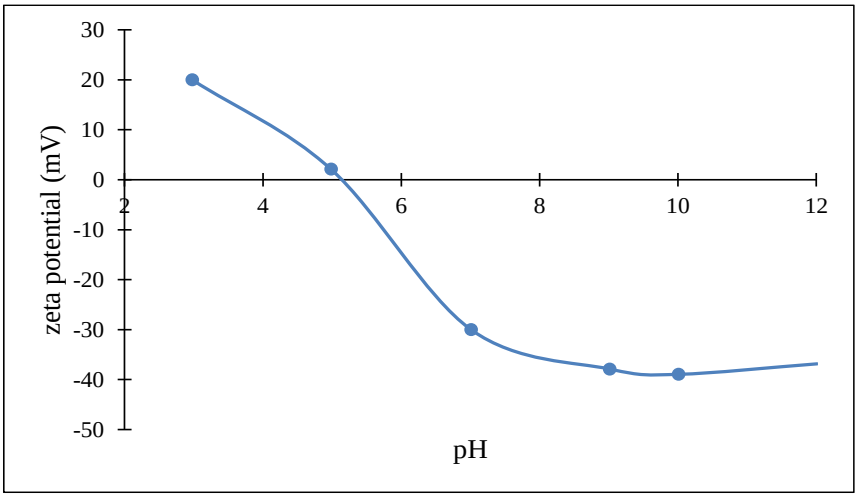

Fig. 14. Variation of zeta potential with pH for slurries containing dispersants

3-3- Effect of dispersant amount

To investigate the effect of Dolapix CE64 concentration on slurry stability, its content was gradually increased relative to the solid fraction of the slurry. All prepared slurries contained 70 wt% alumina powder. Fig. ***15***illustrates the effect of Dolapix CE64 addition on the sediment percentage after 24 hours. The lowest sedimentation corresponds to the most stable slurry.

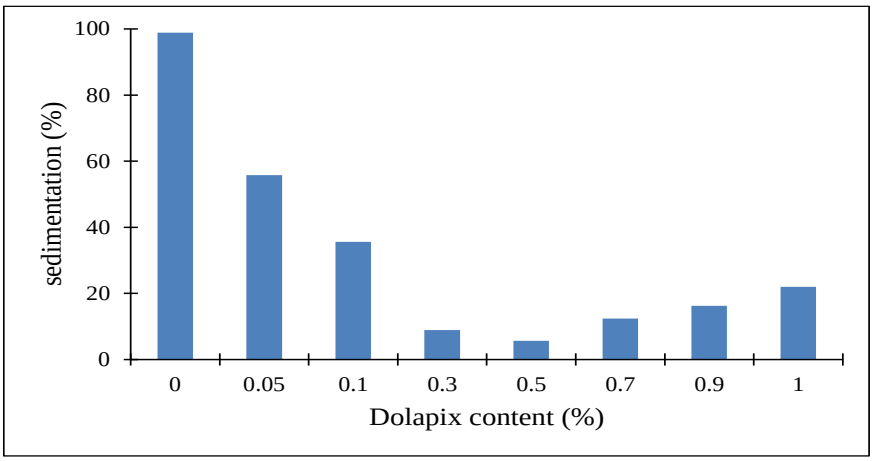

Fig. 15. Sedimentation percentage of the slurry after 24 hours as a function of Dolapix CE64 concentration

As shown in Fig. 15, slurries containing 0.3–0.5 wt% Dolapix CE64 exhibited the lowest sedimentation. In slurries with dispersant content below this optimal range, the alumina particles are not fully covered, allowing Van der Waals forces to dominate, leading to flocculation and increased sediment formation. Conversely, in slurries with more than 0.5 wt% Dolapix CE64, the excess dispersant that is not adsorbed onto particle surfaces remains in the liquid phase, acting as an electrolyte, which compresses the electric double layer and promotes agglomeration. Therefore, it can be concluded that slurries containing 0.3–0.5 wt% Dolapix CE64 achieve the highest zeta potential, minimizing the likelihood of agglomeration and sedimentation. In practice, the optimal slurry for aluminum foam formation is one in which the dispersant is fully adsorbed onto particle surfaces, with no free dispersant remaining in the liquid phase, ensuring a homogeneous and stable suspension.

3-4- Achieving alumina foam with optimal properties

In this stage of the process, the stabilized slurry containing the dispersant was introduced into the foaming system, where it was aerated by injecting air. Subsequently, silica sol and magnesium oxide were added to convert the aerated slurry into a wet gel, which was then dried and sintered. In this phase, the factors influencing the properties of the final product were systematically investigated. The ultimate goal was to produce a sample that combines high mechanical strength with low density.

According to Fig. 16, colloidal silica was employed to convert the aerated alumina slurry into a wet gel. The internal structure of colloidal silica particles

consists of siloxane networks (-Si–O–Si-), while their surface is covered with numerous silanol (-SiOH)$^-$ and hydroxyl (-OH)$^-$ groups. Gelation occurs when siloxane bonds are formed on the surface of the nanoparticles through the condensation of silanol groups as presented in Eq. (4) [20].

$$(-SiOH)^- + (HOSi-)^- \rightarrow (-SiOSi-) + H_2O \quad (4)$$

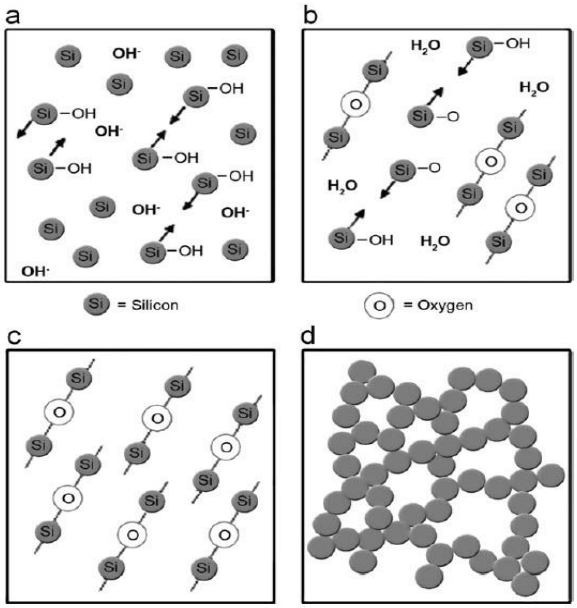

Fig. 16. Gelation mechanism of colloidal silica [21]

Sintered magnesia powder has frequently been used as a binding additive in the literature [22]. Magnesia typically participates in anionic reactions by forming magnesium hydroxide, and through the release of hydrogen ions from Si–OH groups, it promotes the formation of additional siloxane bonds, thereby increasing the gelation rate of colloidal silica as depicted in Fig. 17. In this study, 4 wt% colloidal silica and 0.6 wt% magnesia were added to the slurry, resulting in samples with sufficient green strength for further processing.

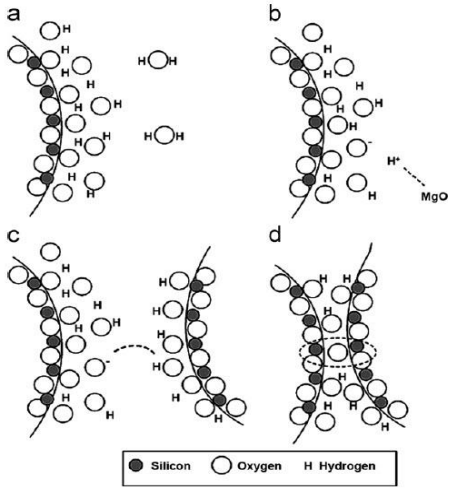

Fig. 17. Schematic of gelation mechanism a) The surface of colloidal silica particles b) Increasing MgO c) Formation of siloxane bond d) Siloxane bonds [21]

The effect of sintering temperature on the density, porosity, and mechanical strength of the manufactured samples is presented in Figure 10. The high compressive strength observed at 1200 °C indicates that colloidal silica can lower the sintering temperature, enabling particle bonding at relatively low temperatures. This behavior is primarily attributed to the nanoscale size of the colloidal silica particles, which enhances the sinterability of the foam system.

Figure 11 shows the variation in bulk density of the foam samples after sintering at different temperatures. Although the compressive strength increases with rising temperature, the porosity and density remain nearly constant up to 1200 °C. Since the setting of colloidal silica is non-hydraulic, the porosity and density are largely insensitive to temperature changes within this range. However, when the sintering temperature exceeds 1200 °C, the density increases and porosity decreases, indicating the progression of the sintering process. Considering that the final samples should possess high strength while maintaining low density, the optimal sintering temperature was determined to be 1400 °C. Accordingly, all subsequent experiments were conducted with samples sintered at this temperature.

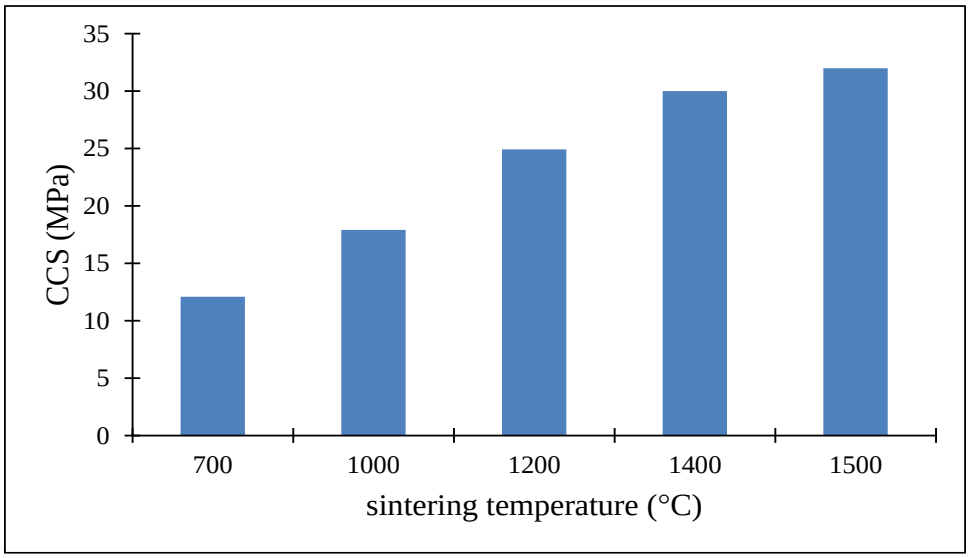

Fig. 18. Cold compressive strength (CCS) of foam samples after curing at different temperatures

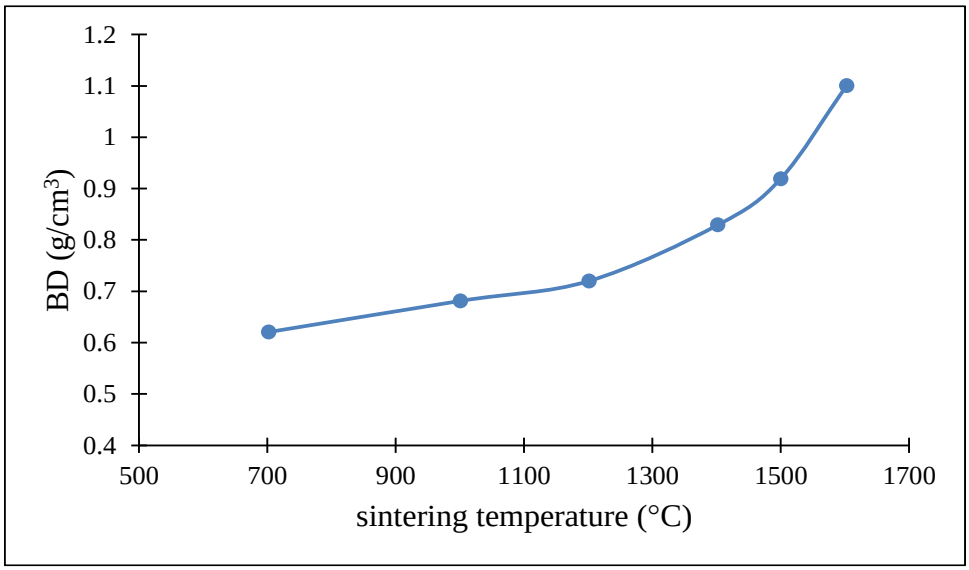

Fig. 19. Body density of foam samples after sintering at different temperatures

To investigate the effect of solid content, slurries with 70, 72, 75, 78, and 80 wt% alumina were prepared and injected into the foaming chamber. The resulting physical properties are presented in Fig. 20 and Fig. 21. It is evident that increasing the solid content leads to higher density and lower porosity. The reduction in porosity can be attributed to the decreased ability to form bubbles as the solid fraction increases. Since bubble formation in the slurry occurs within the liquid phase, increasing the solid content reduces the amount of liquid available, thereby decreasing bubble formation and, consequently, the porosity of the final product. This reduction in porosity results in higher density. Density plays a critical role in determining the microstructure of the sintered parts. As shown in Fig. 22, SEM images of sintered samples with varying densities reveal that pore size decreases with increasing density.

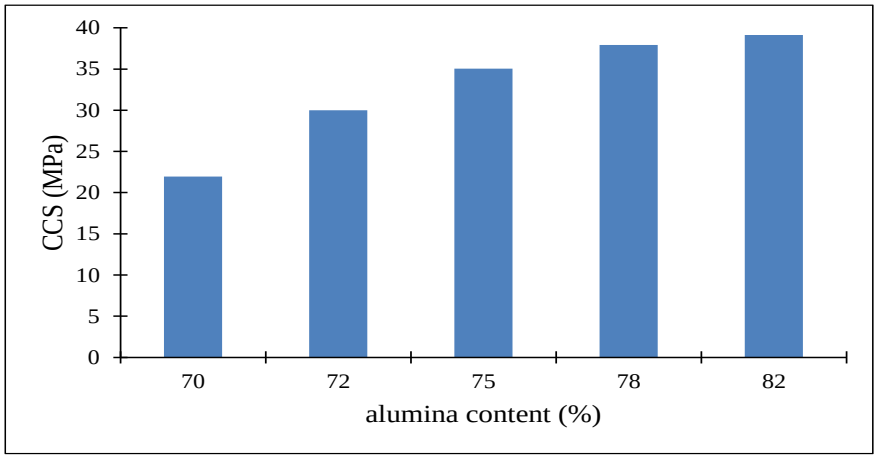

Fig. 20. Cold compressive strength (CCS) of foam samples at different alumina contents

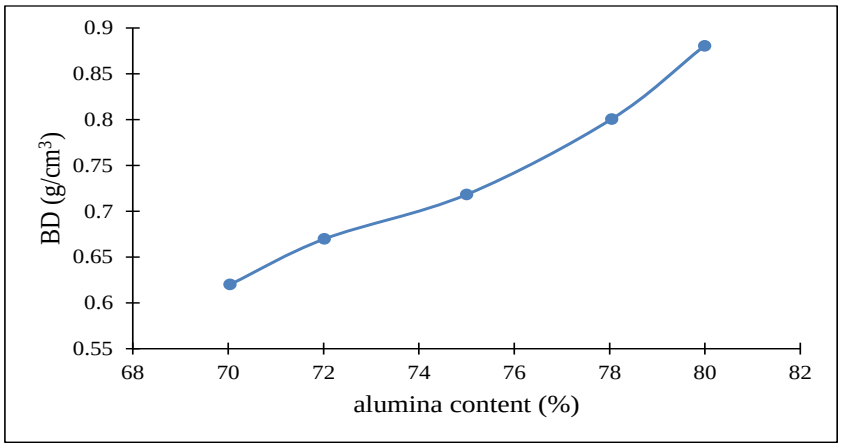

Fig. 21. Body density of foam samples at different alumina contents

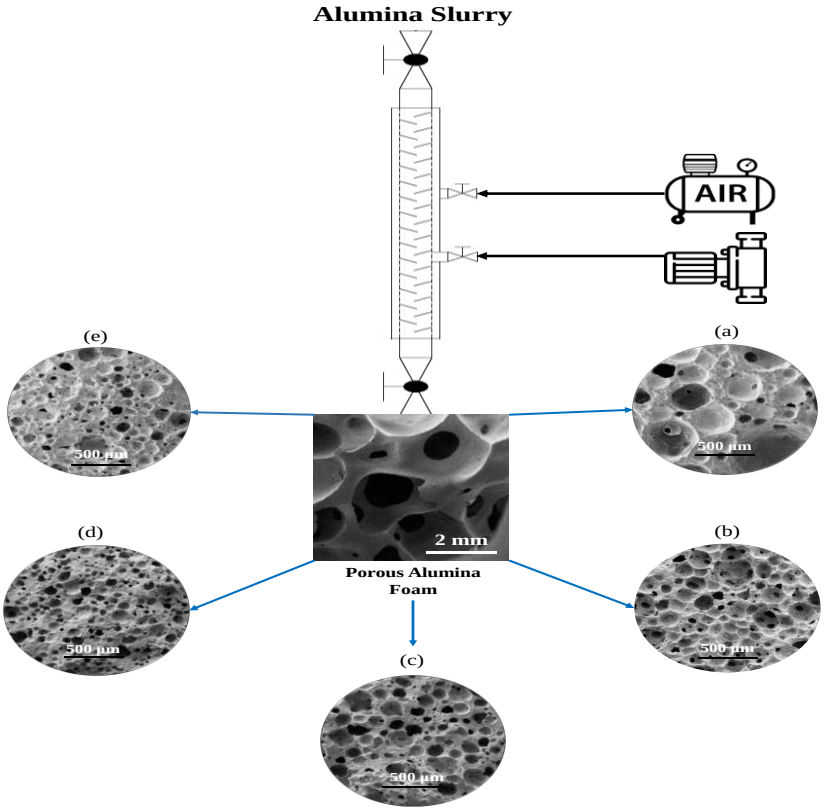

Fig. 22. SEM images of porous bodies with solid percentages a) 70 b) 72 c) 75 d) 78 and e) 80 percent by weight of alumina

Based on the above investigations, the sample containing 78 wt% solids, sintered at the optimal temperature of 1400 °C, exhibited the best combination of properties, achieving both low density and adequate mechanical strength. Finally, according to Table 2 a comparison between the optimized sample and other manufactured samples was conducted, demonstrating that the resulting parts possess similar properties and confirming the reproducibility of the fabrication process.

Table 2. Comparison of the properties of the reference sample and the optimized sample

Characteristics	Density (g/cm^3)	Cold compressive strength (Mpa)	Porosity (%)	Heat conduction (W/m.K)
Reference sample	0.85	35	85	0.56
Optimized sample	0.92	30	78	0.7

4- Conclusion

In this paper, Dolapix CE64 was used as a dispersant to stabilize 70% by weight slurry prepared from alpha alumina powder, and it was found that by adding 0.3% of Dolapix CE64, a stable slurry can be prepared. The results of the tests related to determining the optimal amount of the dispersant were in significant agreement with the results of the rheometric test. By increasing the solid percentage of the slurry for foam production, the density and strength values increase and the porosity and the average size of the pores decrease. In this project, a colloidal silica binder (silica sol) was used as a binding agent and gelation was done with the addition of magnesium oxide. As the sintering temperature increases, the density and strength increase due to the progress of the sintering process.

References

[1] I. Finhana, O. Borges, T. Santos Jr, V. Salvini, and V. Pandolfelli, "Direct foaming of Al2O3-based macroporous ceramics containing pre-foamed colloidal alumina, calcite and CAC suspension", Ceram. Int., Vol. 47, 2021, pp. 22717-22724.

[2] F. Xia, S. Cui, and X. Pu, "Performance study of foam ceramics prepared by direct foaming method using red mud and K-feldspar washed waste", Ceram. Int., Vol. 48, 2022, pp. 5197-5203.

[3] X. Li, S. Li, Y. Li, S. Li, P. Chen, and T. Guo, "Fabrication of novel BPO4 ceramic foams using the combination of the direct foaming method and freeze-drying techniques", Int. J. App. Ceram. Tech., Vol. 20, 2023, pp. 3565-3575.

[4] L.-y. Zhang, D.-l. Zhou, Y. Chen, B. Liang, and J.-b. Zhou, "Preparation of high open porosity ceramic foams via direct foaming molded and dried at room temperature", J. Eur. Ceram. Soc., Vol. 34, 2014, pp. 2443-2452.

[5] V. C. Colonetti, M. F. Sanches, V. C. de Souza, C. P. Fernandes, D. Hotza, and M. G. N. Quadri, "Cellular ceramics obtained by a combination of direct foaming of soybean oil emulsified alumina suspensions with gel consolidation using gelatin", Ceram. Int., Vol. 44, 2018, pp. 2436-2445.

[6] Z. Guo, L. An, S. Lakshmanan, J. N. Armstrong, S. Ren, and C. Zhou, "Additive manufacturing of porous ceramics with foaming agent", J. Manuf. Sci. Eng., Vol. 144, 2022, p. 021010.

[7] T. Ohji and M. Fukushima, "Macro-porous ceramics: processing and properties", Int. Mater. Rev., Vol. 57, 2012, pp. 115-131.

[8] C. Wang, J. Wang, Q. Li, S. Xu, and J. Yang, "A review on recent development of foam Ceramics prepared by particle-stabilized foaming technique", Adv. Colloid Interface. Sci., Vol. 330, 2024, p. 103198.

[9] Q. Leng, D. Yao, Y. Xia, H. Liang, and Y.-P. Zeng, "Microstructure and permeability of porous zirconia ceramic foams prepared via direct foaming with mixed surfactants", J. Eur. Ceram. Soc., Vol. 42, 2022, pp. 7528-7537.

[10] X. Zhang, X. Zhang, X. Li, and M. Ma, "Bubble behaviors in chemical direct foaming process and effects on pore structures of geopolymer foams", J. Am. Ceram. Soc., Vol. 105, 2022, pp. 6063-6075.

[11] C. Zhao, C. Wang, Z. Xia, C. Jiang, Y. Dong, and Z. Lan, "Effect of Various Foaming Agents on Ceramic Foam from Solid Waste", Crystals, Vol. 15, 2024, p. 32.

[12] I. C. Finhana, V. V. S. Machado, T. Santos, O. H. Borges, V. R. Salvini, and V. C. Pandolfelli, "Direct foaming of macroporous ceramics containing colloidal alumina", Ceram. Int., Vol. 47, 2021, pp. 15237-15244.

[13] A. R. Studart, U. T. Gonzenbach, E. Tervoort, and L. J. Gauckler, "Processing routes to macroporous ceramics: a review", J. Am. Ceram. Soc., Vol. 89, 2006, pp. 1771-1789.

[14] S. Barg, D. Koch, and G. Grathwohl, "Processing and properties of graded ceramic filters", J. Am. Ceram. Soc., Vol. 92, 2009, pp. 2854-2860.

[15] I. Capasso, "Design and Synthesis of Hybrid Ceramic Foams with Tailored Porosity," PhD, University of Naples Federico II, 2017.

[16] D. Werner, J. Maier, N. Kaube, V. Geske, T. Behnisch, M. Ahlhelm, *et al.*, "Tailoring of

hierarchical porous freeze foam structures", Materials, Vol. 15, 2022, p. 836.

[17] H. Lu, Y. Li, D. Liu, D. Sun, Y. You, E. Jin, *et al.*, "Effects of slurry solid loading and molar ratio of CaO to Al2O3 on the properties of direct foamed porous calcium hexaluminate (CA6) ceramics", Ceram. Int., Vol. 51, 2025, pp. 29400-29408.

[18] S. Kirchhof, A. Ams, and G. Hütter, "On the question of the sign of size effects in the elastic behavior of foams", J. elast., Vol. 156, 2024, pp. 79-93.

[19] A. Shimamura, "A review on gradient macroporous ceramic via powder-based direct foaming process", J. Ceram. Soc. Jpn., Vol. 130, 2022, pp. 204-210.

[20] I. S. Martinatti, "Studies on high-alumina colloidal silica-bonded refractory castable systems," Universidade de SÃ£ o Paulo, 2024.

[21] I. M. I. Bayoumi, E. M. M. Ewais, and A. A. M. El-Amir, "Rheology of refractory concrete: An article review", Boletín de la Sociedad Española de Cerámica y Vidrio, Vol. 61, 2022, pp. 453-469.

[22] M. Salehi, K. X. Kuah, Z. Huang, D. J. Blackwood, S. X. Zhang, H. L. Seet, *et al.*, "Enhancing densification in binder jet additive manufacturing of magnesium via nanoparticles as sintering aids", J. Manuf. Proc., Vol. 99, 2023, pp. 705-717.